Migration velocity analysis for TI media with quadratic lateral velocity variation

Mamoru Takanashi[1,2] & Ilya Tsvankin[1]

[1] *Center for Wave Phenomena, Geophysics Department, Colorado School of Mines, Golden, Colorado 80401*
[2] *Japan Oil, Gas and Metals National Corporation, Chiba, Japan*

ABSTRACT

One of the most serious problems in anisotropic velocity analysis is the trade-off between anisotropy and lateral heterogeneity, especially if velocity varies on a scale smaller than spreadlength. Here, we develop a P-wave MVA (migration velocity analysis) algorithm for transversely isotropic (TI) models that include layers with small-scale lateral heterogeneity. Each layer is described by constant Thomsen's parameters ϵ and δ and the symmetry-direction velocity V_0 that varies as a quadratic function of the distance along the layer boundaries. For tilted TI media (TTI), the symmetry axis is taken orthogonal to the reflectors. We analyze the influence of lateral heterogeneity on image gathers obtained after prestack depth migration and show that quadratic lateral velocity variation in the overburden can significantly distort the moveout of the target reflection. If such errors are not corrected, the medium parameters beneath the heterogeneous layer(s) are estimated with significant error, even when borehole information (e.g., check shots or sonic logs) is available. Since the residual moveout is highly sensitive to lateral heterogeneity in the overburden, our algorithm simultaneously inverts for the parameters of all layers or blocks. Synthetic tests demonstrate that if the vertical profile of the symmetry-direction velocity V_0 is known at one location, the algorithm can reconstruct the other relevant parameters throughout the medium. The developed method should increase the robustness of anisotropic velocity model-building and image quality in the presence of laterally heterogeneous layers in the overburden.

Key words: MVA, VTI, TTI, quadratic lateral velocity variation, factorized media

1 INTRODUCTION

Anisotropic parameter estimation has become an essential part of a wide range of seismic-imaging and reservoir-characterization projects (e.g. Tsvankin et al., 2010). Ignoring anisotropy can lead to mispositioning of horizontal and dipping reflectors, poor focusing of dipping events, etc. (Alkhalifah and Larner, 1994; Alkhalifah, 1997). Migration velocity analysis (MVA) has been extended to heterogeneous transversely isotropic media with a vertical (VTI) and tilted (TTI) symmetry axis (e.g. Sarkar and Tsvankin, 2004; Biondi, 2007; Behera and Tsvankin, 2009; Bakulin et al., 2010b,c). Numerous field examples demonstrate that application of prestack depth migration (PSDM) with anisotropic MVA yields significantly improved images for TI models (Huang et al., 2008; Calvert et al., 2008; Neal et al., 2009; Bakulin et al., 2010a).

However, anisotropic velocity analysis suffers from trade-offs between anisotropy parameters, lateral velocity variation, and the shapes of the reflecting interfaces. To make parameter estimation more stable, existing algorithms often keep the anisotropy parameters ϵ and/or δ fixed during iterative parameter updates.

Sarkar and Tsvankin (2003,2004) present a 2D MVA algorithm designed to estimate both the spatially varying velocity and parameters ϵ and δ of VTI media. They divide the model into factorized blocks, in which the ratios of the stiffness coefficients c_{ij} and, therefore, the anisotropy parameters are constant. The vertical velocity V_0 in each factorized block can vary in arbitrary fashion with the spatial coordinates (Červený, 1989),

but Sarkar and Tsvankin (2003,2004) employ the simplest, linearly varying $V_0(x,\, z)$ field:

$$V_0(x,\, z) \quad = \quad V_0(0,0) + k_{x1}\, x + k_{z1}\, z\,, \tag{1}$$

where k_{x1} and k_{z1} are the horizontal and vertical velocity gradients, respectively. If V_0 is known at a single point in each factorized VTI block, the MVA algorithm can estimate the parameters ϵ and δ along with the velocity gradients. Two reflectors in each block, sufficiently separated in depth, are required for constraining k_{z1}. It is also essential to use long-spread data (the spreadlength-to-depth ratio should reach at least two) or dipping events to estimate ϵ (or the anellipticity parameter η). Application of this algorithm to a data set from West Africa produces a higher-quality image and more accurate velocity field compared with that generated by anisotropic *time* processing (Sarkar and Tsvankin, 2006). Behera and Tsvankin (2009) extend this algorithm to "quasi-factorized" TTI media under the assumption that the symmetry axis is orthogonal to the reflector beneath each layer. Because the symmetry-axis orientation generally varies with the shape of the interface, blocks are not "fully" factorized.

Existing methods, however, are designed for relatively large-scale lateral heterogeneity. Lateral velocity variation on a scale comparable to or smaller than spreadlength, often associated with velocity lenses, can distort the estimated parameters and reduce the quality of stack (Al-Chalabi, 1979; Toldi, 1989; Blias, 2009; Takanashi and Tsvankin, 2010). In principle, both lateral and vertical heterogeneity can be handled by anisotropic grid-based reflection tomography (Woodward et al., 2008; Bakulin et al., 2010b,c). However, small-scale lateral heterogeneity may produce significant error in iterative tomographic inversion (Takanashi et al., 2009). Indeed, even if tomography is restricted to the vicinity of a borehole, and the vertical velocity V_0 and reflector dips at the borehole location are known, the results may still remain nonunique (Bakulin et al., 2010b,c).

To properly account for small-scale lateral heterogeneity, we extend the MVA algorithms of Sarkar and Tsvankin (2004) and Behera and Tsvankin (2009) to TI media with quadratic lateral variation of the symmetry-direction velocity V_0. The model is composed of "quasi-factorized" TI blocks with constant ϵ and δ and the symmetry axis orthogonal to the reflectors. First, we show that quadratic lateral velocity variation in a thin layer in the overburden leads to residual moveout and distortions in parameter estimation for the target interval. To exploit the sensitivity of residual moveout to small-scale lateral heterogeneity in the overburden, we devise an MVA algorithm that simultaneously estimates the medium parameters for all layers or blocks. Synthetic tests demonstrate that our method can accurately reconstruct the velocity field for TI models with thin laterally heterogeneous layers, if some a priori information about the symmetry-direction velocity is available.

2 INFLUENCE OF QUADRATIC LATERAL VELOCITY VARIATION ON IMAGE GATHERS

First, we analyze the influence of lateral velocity variation on the scale of spreadlength for a piecewise-factorized VTI model. By adding a quadratic term in x to equation 1, the vertical velocity V_0 in each block takes the form:

$$V_0(x,\, z) = V_0(0,0) + k_{x1}\, x + k_{z1}\, z + k_{x2}\, x^2\,. \tag{2}$$

A smooth (e.g., parabola-shaped) low-velocity lens centered at $x = 0$ can be approximated by the velocity function $V_0(x,\, z)$ with a positive k_{x2}. Likewise, a high-velocity lens can be characterized by a negative k_{x2}.

Takanashi and Tsvankin (2011a,b) discuss the influence of thin laterally heterogeneous (LH) layers on the reflection moveout from deeper interfaces. They show that the distortion of the NMO velocity or ellipse depends on the curvature of the vertical interval traveltime, and the magnitude of the distortion increases with the distance between the LH layer and the target. When lateral heterogeneity is confined to the middle layer, the NMO velocity at the bottom of a horizontal three-layer model becomes (Takanashi and Tsvankin, 2011b):

$$V_{\rm nmo,het}^{-2} = V_{\rm nmo,hom}^{-2} + \frac{\tau_0\, D}{3}\, \frac{\partial^2 \tau_{02}}{\partial x^2}\,, \tag{3}$$

$$D = k^2 + 3k\, l + 3l^2, \tag{4}$$

where $V_{\rm nmo,het}$ is the NMO velocity in the presence of lateral velocity variation, and $V_{\rm nmo,hom}$ is the NMO velocity for the reference laterally homogeneous medium with the parameters corresponding to the same location. τ_0 is the zero-offset traveltime and τ_{02} is the zero-offset interval traveltime for the second layer. The coefficient D is determined by the parameters k and l, which are close to the relative thicknesses of the second and third layer, respectively, if the vertical velocity variation is small (Takanashi and Tsvankin, 2011b).

Under the assumption that the model is horizontally layered and lateral heterogeneity is weak, the second derivative of the vertical traveltime can be replaced with that of the vertical velocity (Grechka and Tsvankin, 1999):

$$\frac{\partial^2 \tau_{02}(x)}{\partial x^2}\, V_{02}(x) + \frac{\partial^2 V_{02}(x)}{\partial x^2}\, \tau_{02}(x) = 0\,, \tag{5}$$

where $V_{02}(x)$ is the vertical velocity in the second layer. If the velocity V_{02} is described by quadratic equation 2, equation 3 can be rewritten as

$$V_{\rm nmo,het}^{-2}(x) = V_{\rm nmo,hom}^{-2}(x) - \frac{2\,\tau_0(x)\,\tau_{02}(x)\, D\, k_{x2}^{(2)}}{3\, V_{02}(x)}, \tag{6}$$

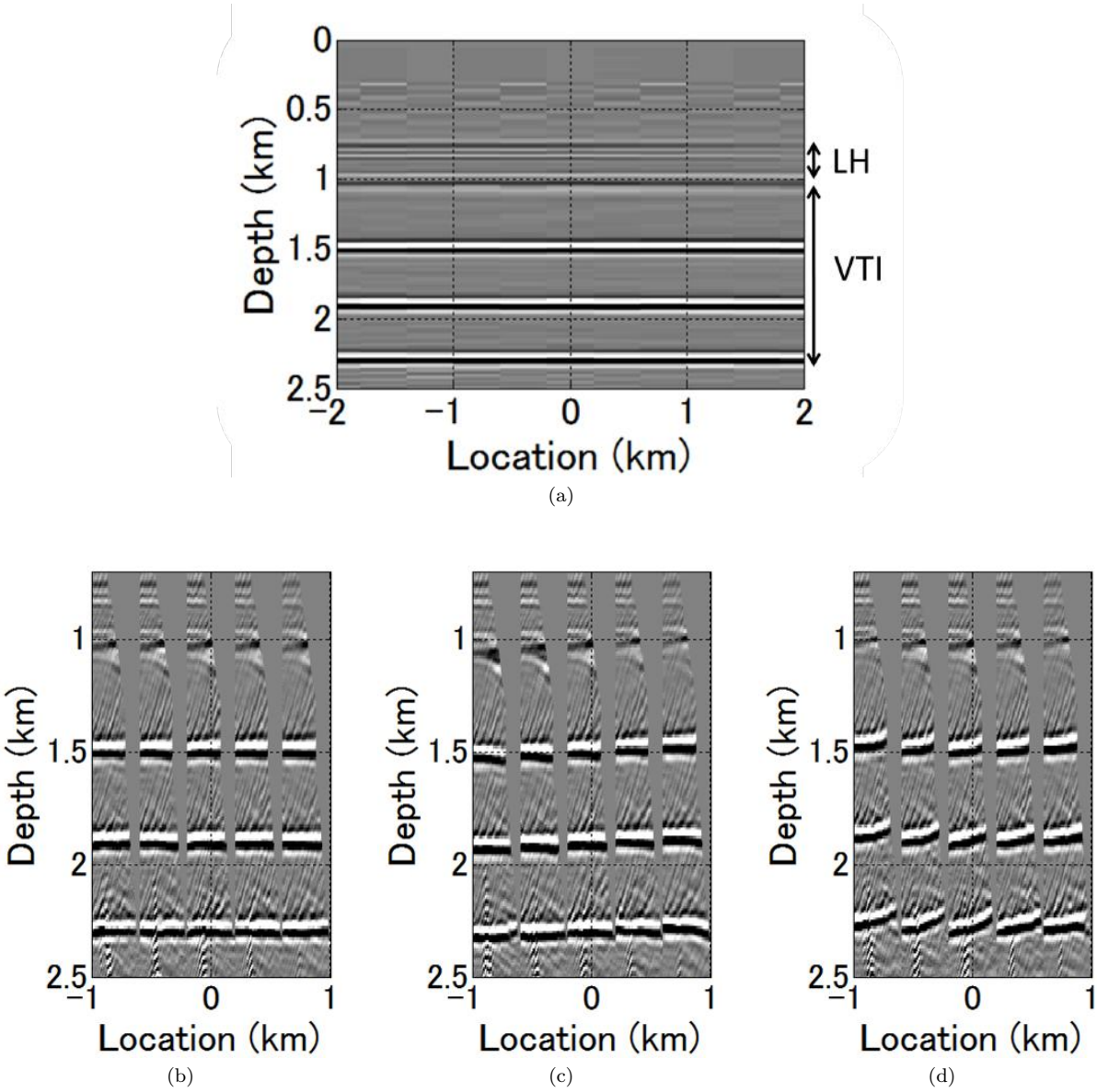

Figure 1. (a) Image of a horizontally layered model obtained by anisotropic prestack depth migration with the actual medium parameters. The top layer is homogeneous and isotropic with $V_0 = 3000$ m/s. The parameters of the LH layer are $V_0(0) = 2280$ m/s, $k_{x1} = 0.24\,\mathrm{s}^{-1}$ and $k_{x2} = 2.4 \times 10^{-4}$ $\mathrm{s}^{-1}\mathrm{m}^{-1}$. The parameters of the VTI medium beneath the LH layer are $V_0 = 3000\,\mathrm{m/s}$, $k_{x1} = 0.1\,\mathrm{s}^{-1}$, $k_{z1} = 0$, $\epsilon = 0.2$, and $\delta = 0.1$. Image gathers produced (b) with the actual parameters; (c) and (d) with an inaccurate parameter of the thin laterally heterogeneous (LH) layer: (c) $k_{x1} = 0$; (d) $k_{x2} = 0$ (the other parameters are correct). The maximum offset is 4 km.

where $k_{x2}^{(2)}$ is the quadratic coefficient for the second layer.

Since $V_{\mathrm{nmo,het}}(x)$ is responsible for conventional-spread moveout, near-offset image gathers become flat when $V_{\mathrm{nmo,het},T}(x) = V_{\mathrm{nmo,het},M}(x)$, where the subscript T refers to the true model and M to the model used for migration. If $k_{x2}^{(2)}$ is positive, neglecting its contribution in equation 6 and identifying the estimated $V_{\mathrm{nmo,het}}$ with $V_{\mathrm{nmo,hom}}$ leads to overstated values of $V_{\mathrm{nmo,hom}}(x)$. Likewise, neglecting a negative $k_{x2}^{(2)}$ (or a high-velocity lens) leads to understated $V_{\mathrm{nmo,hom}}(x)$.

The $k_{x2}^{(2)}$-related distortion in the effective NMO velocity increases with target depth because both τ_0 and D become larger (Takanashi and Tsvankin, 2011b). Thus, the moveout in image gathers for deep reflectors is highly sensitive to errors in k_{x2} in the overburden.

Also, the influence of k_{x2} distorts the interval NMO velocity (or δ if the vertical velocity is known) in the third layer. Note that a constant lateral velocity gradient does not significantly influence the NMO velocity for deeper events, as indicated by the absence of the gradient $k_{x1}^{(2)}$ in equation 6.

The synthetic results of Takanashi and Tsvankin (2010) also show that velocity lenses in the overburden cause errors in the anellipticity parameter η obtained from nonhyperbolic moveout inversion. According to the analytic results of Grechka (1998), the estimated η depends on second and fourth lateral derivatives of the vertical velocity and, therefore, on k_{x2}.

The influence of errors in k_{x1} and k_{x2} in a thin layer on image gathers obtained after Kirchhoff prestack depth migration is illustrated by Figure 1. Prestack synthetic data are produced by a finite-difference algorithm (using the Seismic Unix code suea2df, Juhlin, 1995). The error in either k_{x1} or k_{x2} leads to a velocity variation of 960 m/s between $x = -2$ km and $x = 2$ km.

Although the error in k_{x1} leads to inaccurate V_0 at $x \neq 0$ and distorts positions of the reflectors, the corresponding residual moveout is relatively small at all depths (Figure 1c). In contrast, ignoring k_{x2} leads to a substantial overcorrection (i.e., the imaged depth decreases with offset) for the reflectors from interfaces far below the thin layer. Consequently, failure to correct for the error in k_{x2} leads to distorted medium parameters at depth. Indeed, iterative application of prestack depth migration and velocity updating without correcting for the influence of small-scale lateral heterogeneity amplifies the residual moveout and parameter errors for deep reflectors (e.g., Takanashi et al., 2009).

2.1 TTI model with quadratic velocity variation

Next, we analyze image gathers for a layered TTI model with quadratic velocity variation. We assume that the symmetry axis is orthogonal to the bottom reflector in each block and that the symmetry-direction velocity V_0 is represented as

$$V_0(\overline{x},\, \overline{z}) = V_0(0,\, 0) + \overline{k}_{x1}\overline{x} + \overline{k}_{z1}\overline{z} + \overline{k}_{x2}\overline{x}^2\,, \qquad (7)$$

where $\overline{x}$ and $\overline{z}$ are the rotated coordinate axes parallel and perpendicular to the layer boundaries (Figure 2). This model may represent channel-filled or turbidite sands embedded in shaly deposits, which are often found in continental slope areas (Contreras and Latimer, 2010; van Hoek et al., 2010).

If the near-surface layer is homogeneous and all layers have close dips, the moveout distortion in image gathers is primarily caused by $\overline{k}_{x2}$ (Figure 3). In contrast, errors in $\overline{k}_{x1}$ do not produce significant residual moveout in image gathers (Figure 3c). Therefore, the coefficients k_{x2} and $\overline{k}_{x2}$ play a key role in velocity analysis for both VTI and TTI media.

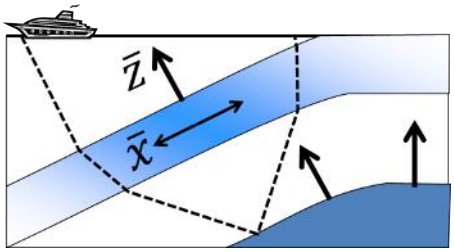

Figure 2. Schematic section of a three-layer TTI model. The symmetry-direction velocity V_0 varies as a quadratic function of the distance along the layer boundaries. The symmetry axis of the TTI layer is perpendicular to its bottom.

3 MVA FOR MODELS WITH QUADRATIC VELOCITY VARIATION

As in conventional MVA algorithm, we iteratively apply PSDM and velocity update until the residual moveout becomes sufficiently small. To estimate the residual moveout for long-offset data, Sarkar and Tsvankin (2004) introduce the following nonhyperbolic equation in the migrated domain:

$$z_M^2(h) \approx z_M^2(0) + Ah^2 + B\frac{h^4}{h^2 + z_M^2(0)}\,, \qquad (8)$$

where z_M is the migrated depth, h is the half-offset, and A and B are dimensionless coefficients responsible for the residual moveout at near and far offsets, respectively. Equation 8 is employed in two-dimensional semblance analysis with the goal of evaluating the magnitude of the residual moveout. In our model, each block is described by the parameters V_0, δ, ϵ, k_{x1}, k_{z1}, and k_{x2} (or $\overline{k}_{x2}$ for TTI models; instead of $\overline{k}_{x1}$ and $\overline{k}_{z1}$, we can operate with k_{x1} and k_{z1}).

Inversion for the parameters of a thin layer in the layer-stripping mode is generally unstable (Sarkar and Tsvankin, 2004). The moveout at the bottom of the thin layer in Figures 1 and 3 is distorted by NMO stretch, which can lead to further instability in the parameter updates. However, the residual moveout of deep events is quite sensitive to errors in the coefficient k_{x2} in the overburden. Therefore, it is beneficial to invert the residual moveout for reflectors at all depths simultaneously, particularly when a model contains quadratic lateral velocity variation.

To make the inversion algorithm of Sarkar and Tsvankin (2004) suitable for such simultaneous parameter update, the perturbations of the migrated depths are expressed as linear functions of the perturbations of the medium parameters in all blocks. Then the velocity updates are implemented using the technique of Sarkar and Tsvankin (2004,Appendix A).

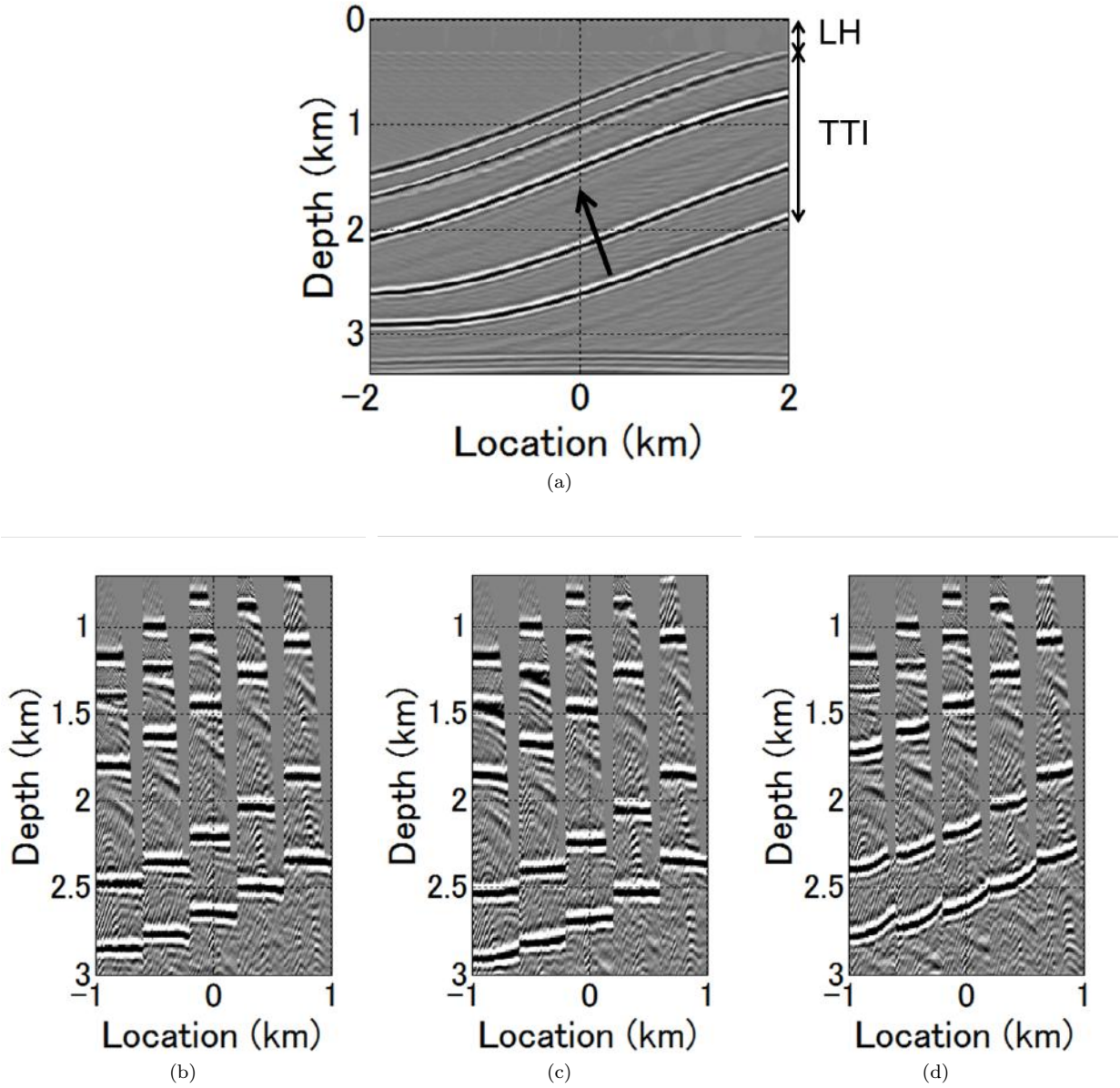

Figure 3. (a) Image of a dipping TTI model (maximum dip of 20°) obtained by anisotropic prestack depth migration with the actual medium parameters. The top layer is homogeneous and isotropic with $V_0 = 3000\,\mathrm{m/s}$. The parameters of the LH layer are $V_0(0) = 2280\,\mathrm{m/s}$, $\overline{k}_{x1} = 0.24\,\mathrm{s}^{-1}$ and $\overline{k}_{x2} = 2.4 \times 10^{-4}\ \mathrm{s}^{-1}\mathrm{m}^{-1}$. The parameters of the TTI medium beneath the LH layer are $V_0 = 3000\,\mathrm{m/s}$, $\overline{k}_{x1} = 0.1\,\mathrm{s}^{-1}$, $\overline{k}_{z1} = 0$, $\epsilon = 0.2$, and $\delta = 0.1$; the symmetry axis is orthogonal to the layer's bottom. Image gathers produced with (b) the actual velocity model, (c) an inaccurate value of $\overline{k}_{x1} = 0$ (the other parameters are correct) and (d) an inaccurate value of $\overline{k}_{x2} = 0$, (the other parameters are correct) in the thin LH layer. The maximum offset is 4.5 km.

4 SYNTHETIC TESTS

4.1 Three-layer VTI model

First, the developed MVA algorithm is tested on a horizontally layered model where quadratic velocity variation is confined to a thin, isotropic middle layer (Figure 4). Three reflectors located below the LH layer are embedded in a factorized VTI halfspace. Figure 4b shows a stacked image obtained after PSDM with the actual model parameters. Kirchhoff migration of synthetic finite-difference data generates an accurate image of all reflectors.

We apply the MVA algorithm to layers 2 and 3 using the actual parameters of layer 1. Image gathers

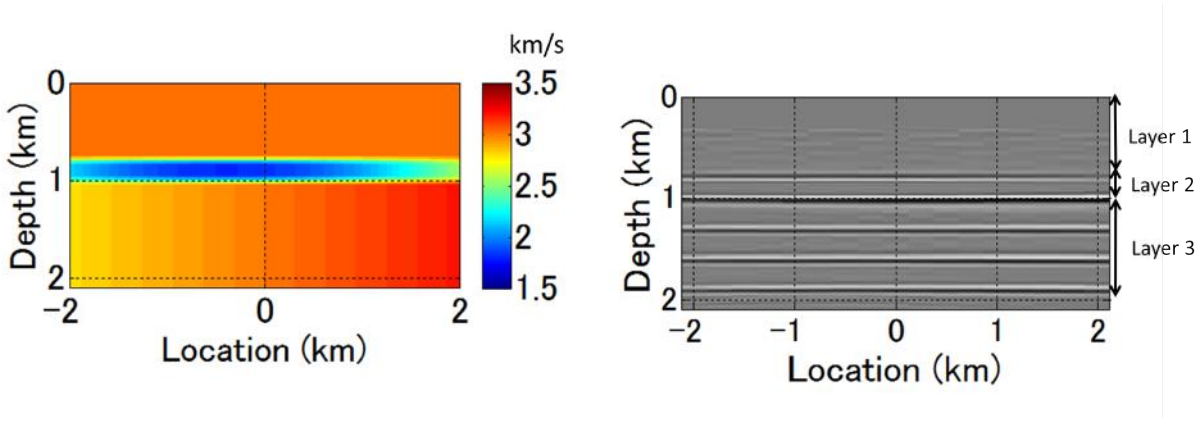

(a) (b)

Figure 4. (a) Model composed of three horizontal layers with quadratic lateral velocity variation in the middle (second) layer. The top layer (Layer 1) is homogeneous and isotropic with $V_0 = 3$ km/s. Layer 2 is isotropic with $V_0 = 1.8$ km/s, $k_{x1} = 0.1\,\mathrm{s}^{-1}$, and $k_{x2} = 1.3 \times 10^{-4}\,\mathrm{s}^{-1}\mathrm{m}^{-1}$. Layer 3 is factorized VTI with $V_0 = 3$ km/s, $k_{x1} = 0.1\,\mathrm{s}^{-1}$, $\epsilon = 0.2$, and $\delta = 0.1$

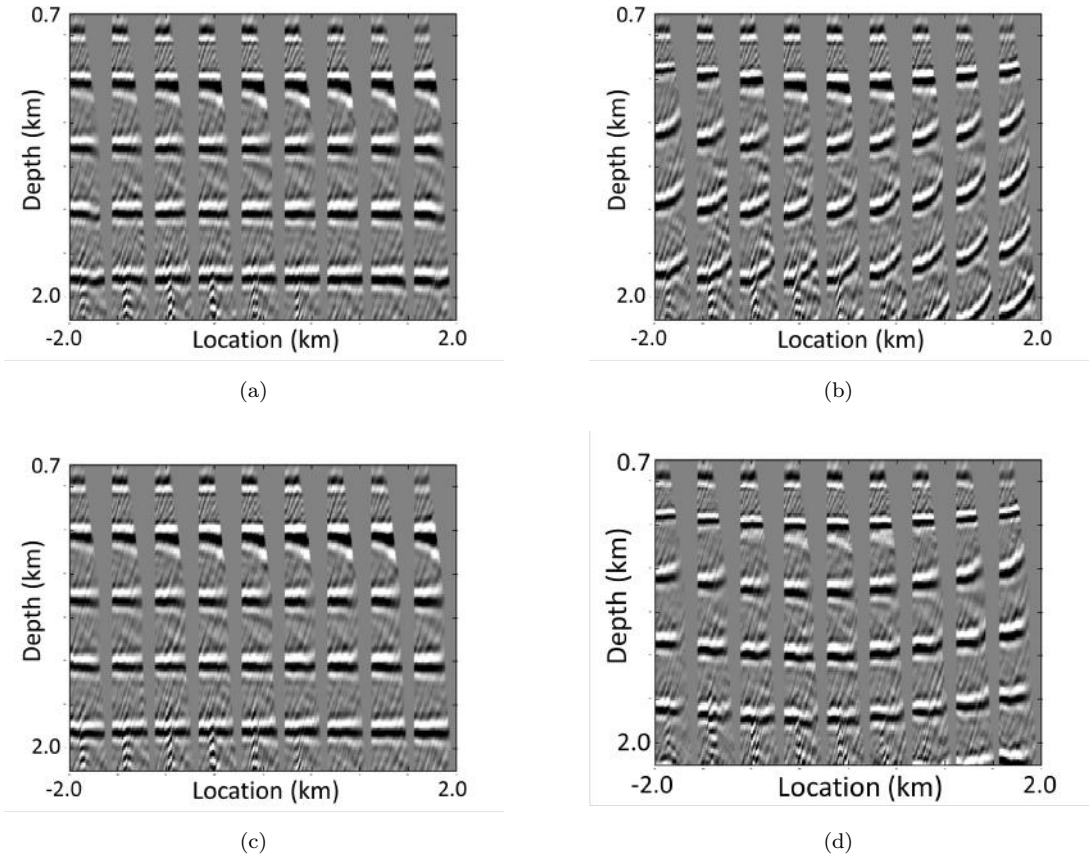

(a) (b)

(c) (d)

Figure 5. Image gathers for the model in Figure 4 obtained with the (a) actual model parameters; (b) laterally homogeneous, isotropic initial model; (c) model estimated by MVA; (d) parameters obtained in the layer-stripping mode with fixed $k_{x2} = 0$ in layers 2 and 3. The maximum offset is 4 km.

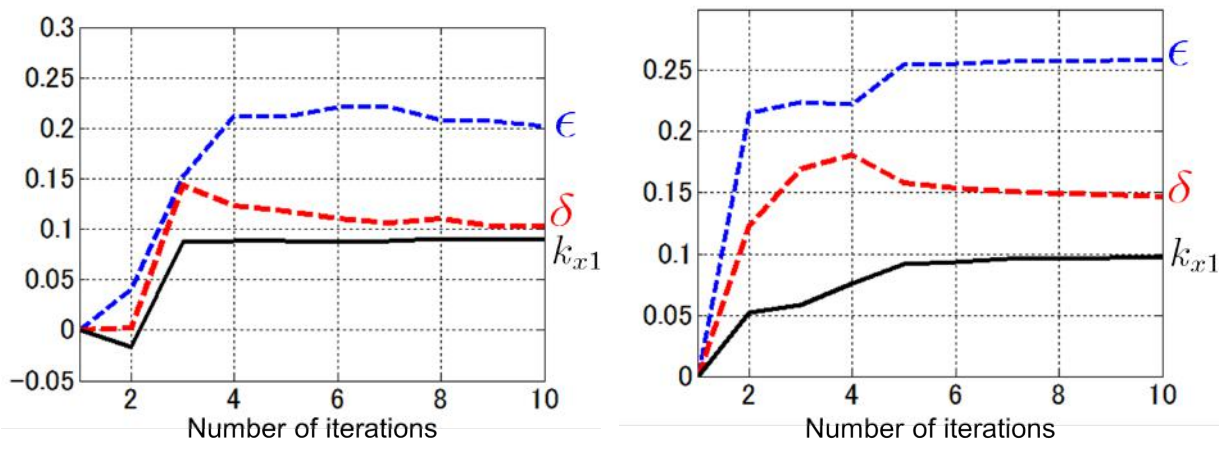

(a) (b)

Figure 6. Estimated parameters of layer 3 for the model from Figure 4 using (a) our algorithm and (b) MVA applied in the layer-stripping mode. The coefficients k_{x2} estimated by algorithm are $1.3 \times 10^{-4}\,\mathrm{s}^{-1}\mathrm{m}^{-1}$ in layer 2 and $6.0 \times 10^{-6}\,\mathrm{s}^{-1}\mathrm{m}^{-1}$ in layer 3.

are produced at horizontal coordinates ranging from -2 km to 2 km with a maximum offset of 4 km. The depth profile of the vertical velocity is assumed to be known at one location ($x = 0$). For example, V_0 and k_{z1} may be found from check shots or sonic logs acquired in a vertical borehole. The initial model is composed of homogeneous, isotropic blocks.

Figure 5b shows image gathers obtained with the initial model parameters. The reflector depths are distorted, and the moveout of the horizontal events in layer 3 is significantly overcorrected. Velocity updating is based on the residual moveout of the three horizontal events in layer 3, which are migrated to incorrect depths. After 10 iterations, the residual moveout for all reflectors is practically eliminated, and the reflectors are properly positioned (Figure 5c). The estimated coefficients k_{x1} and k_{x2} for layer 2, as well as the parameters of layer 3, are close to the actual values (Figure 6a). These results confirm that the residual moveout of deep reflectors can be used to constrain the coefficient k_{x2} in a thin shallow layer.

For comparison, we apply the layer-stripping method of Sarkar and Tsvankin (2004). The value of k_{x2} is set to zero because the velocity variation in each layer has to be linear. The residual moveout after parameter updating is only slightly greater than that in Figure 5c. However, the positions of the reflectors are inaccurate and the estimated values of ϵ and δ in layer 3 are overstated by 0.05 and 0.06, respectively (Figure 6b). The results indicate that the traveltime distortion caused by the inaccurate k_{x2} in layer 2 is largely compensated by distorted parameters in layer 3.

4.1.1 Influence of noise

The influence of random noise on MVA results for TI media is evaluated in Sarkar and Tsvankin (2004) and Behera and Tsvankin (2009). They conclude that even relatively strong random noise is suppressed by prestack migration and does not significantly distort parameter estimates. However, velocity analysis may be sensitive to correlated traveltime errors (Grechka and Tsvankin, 1998; Takanashi and Tsvankin, 2010). Following the approach employed by Wang and Tsvankin (2009), we evaluate the influence of the correlated errors on our algorithm using the prestack data for the model in Figure 4 contaminated with a sinusoidal time function [$t = A\sin(n\pi x/x_{\max})$, where $x_{\max}$ is the maximum offset].

The inverted parameters are more significantly distorted for small values of n (Table 1). Such errors are typically caused by inaccurate statics correction or failure to identify velocity lenses. In agreement with the results of Sarkar and Tsvankin (2004), uncorrelated traveltime errors have little influence on the output of MVA because they are largely removed by semblance analysis (equation 8).

4.1.2 Influence of depth and number of reflectors

It is also important to study the dependence of inversion results on the depth and number of available reflectors in the VTI halfspace. The errors in the estimated parameters somewhat increase with the distance between layer 2 and the shallowest reflector due to the trade-off between the parameters of layers 2 and 3, but the inversion remains well-constrained for all reflector com-

Parameters of error function	A = 8 ms, n=1	A = 8 ms, n=2	A = 8 ms, n=8
Error in δ	0.05	0.01	0.00
Error in ϵ	0.05	0.05	0.02
Error in k_{x1} (s^{-1})	0.01	0.00	0.00

Table 1. Influence of correlated traveltime errors on the estimated parameters of layer 3 for the model in Figure 4. A sinusoidal error function [$t = A\sin(n\pi x/x_{\max})$] was added to each prestack trace.

Reflector depths (km)		1.3, 1.6	1.6, 1.9	1.3, 1.9, 2.5	1.3, 1.9, 2.5 (k_{z1} unknown)
Layer 2	Error in k_{x2} ($s^{-1}m^{-1} \times 10^{-5}$)	3.9	5.7	1.1	5.8
Layer 3	Error in δ	0.02	0.04	0.00	0.05
	Error in ϵ	0.00	0.02	0.01	0.03
	Error in k_{x1} (s^{-1})	0.01	0.01	0.00	0.01
	Error in k_{z1} (s^{-1})	-	-	-	0.15
	Error in k_{x2} ($s^{-1}m^{-1} \times 10^{-5}$)	0.7	1.1	0.2	0.2

Table 2. Estimated parameters of layers 2 and 3 for the model in Figure 4 for different sets of reflectors used in MVA. The results in the right column are obtained without knowledge of the vertical gradient k_{z1} in layer 3.

binations. However, MVA results become less accurate if the vertical gradient k_{z1} in layer 3 is unknown; even when three reflectors well-separated in depth are available, errors in δ and ϵ reach 0.05 and 0.03, respectively (Table 2), and the reflector positions are distorted.

4.2 Multilayered TTI model

Finally, the algorithm is applied to a multilayered TTI model (Table 3) with quadratic velocity variation in two thin isotropic layers at depths of 0.7 km and 1.5 km (for $x = 0$, Figure 7). The thin layers are divided into blocks with a width of 3 km. Using residual moveout for all reflectors, we invert for V_0, k_{x1}, and $\overline{k}_{x2}$ in the thin layers and for k_{x1}, $\overline{k}_{x2}$, ϵ, and δ in the TTI layers. Although for TTI media the symmetry-direction velocity V_0 cannot be obtained directly in a vertical borehole (Wang and Tsvankin, 2010), V_0 profile at location $x = 0$ is assumed to be known for purposes of this test. After 30 iterations, MVA practically removes the residual moveout for all events and accurately recovers the parameters of both isotropic and TTI layers. The errors in δ, ϵ, and k_{x1} in the TTI layers are less than 0.01, 0.03, and 0.01, respectively (Table 3).

Next, we apply the algorithm with the value of $\overline{k}_{x2}$ set to zero. The thin layers are subdivided into smaller blocks (1.5 km wide). The velocity variations in the thin layers are well-resolved and the errors in the parameters of the TTI layers are just slightly higher than those in the previous test. In contrast, running MVA in the layer-stripping mode leads to relatively large residual moveout and significant errors in the TTI parameters (Table 3). The instability of parameter estimation in the layer-stripping mode is partially caused by the NMO stretch at the bottom of the thin LH layers (Figure 8).

5 CONCLUSIONS

In the first part of the paper, we analyzed the influence of small-scale lateral velocity variation in thin layers on P-wave image gathers for VTI and TTI media. The symmetry axis in TTI layers is fixed in the direction orthogonal to the reflectors. Analytic and numerical results demonstrate that the quadratic variation of the symmetry-direction velocity V_0 (controlled by the coefficient k_{x2}) strongly influences the residual moveout for deeper reflectors and can lead to serious distortions in the parameters of the target layer.

To account for heterogeneity on a scale smaller than spreadlength, we extended migration velocity analysis to TI models with quadratic lateral velocity variation. The MVA algorithm simultaneously inverts for the parameters of all blocks or layers, which helps constrain the coefficient k_{x2} in the overburden. Since the k_{x2}-induced errors in the NMO velocity gradually increase with depth, stable parameter estimation generally requires information about of the vertical velocity gradient k_{z1}. Under the assumption that the vertical profile of the symmetry-direction velocity is known at one location in each block, the algorithm accurately reconstructs the laterally-varying velocity fields and anisotropy pa-

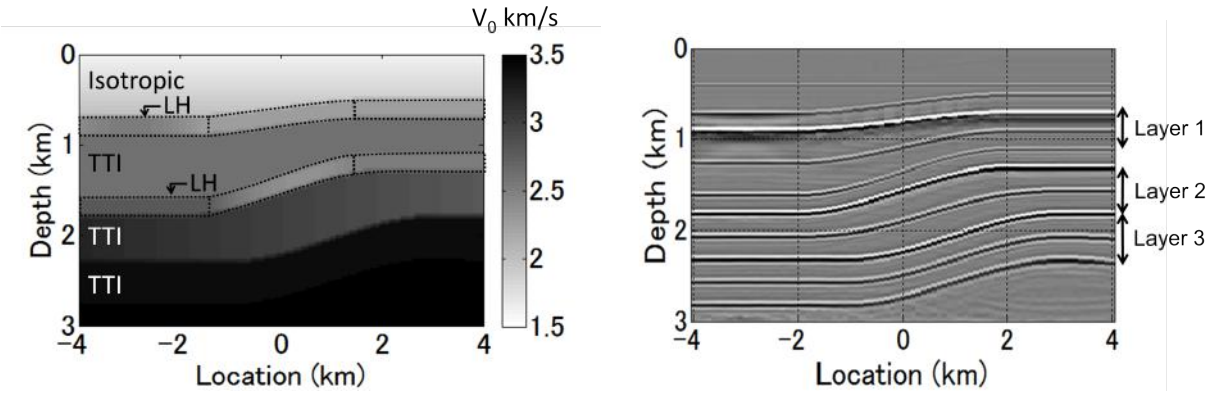

(a) (b)

Figure 7. (a) Multilayered TTI model used in numerical testing. The top layer is isotropic and laterally homogeneous with $V_0(z=0)=1.6$ km/s and $k_{z1}=0.5\,\mathrm{s}^{-1}$. Two thin layers located at 0.7 km and 1.5 km (at $x=0$) are isotropic and vertically homogeneous, but laterally heterogeneous (LH) with quadratic lateral velocity variation. The medium parameters in the TTI layers are listed in Table 3. (b) Image after anisotropic prestack depth migration with the actual model parameters.

		Actual parameters	Full MVA	MVA without $\overline{k}_{x2}$	MVA in layer stripping mode
Layer 1	$V_0(0)$ (km/s)	2.6			
	δ	0.1	0.10	0.11	0.09
	ϵ	0.2	0.23	0.17	0.27
	$k_{x1}(\mathrm{s}^{-1})$	0	0.00	0.03	0.03
	$\overline{k}_{x2}$ $(\mathrm{s}^{-1}\mathrm{m}^{-1}\times 10^{-5})$	0	-1.4		
Layer 2	$V_0(0)$ (km/s)	3.5			
	δ	0.1	0.11	0.13	0.21
	ϵ	0.2	0.18	0.22	0.10
	$k_{x1}(\mathrm{s}^{-1})$	-0.05	-0.055	-0.04	-0.10
	$\overline{k}_{x2}$ $(\mathrm{s}^{-1}\mathrm{m}^{-1}\times 10^{-5})$	0	0.5		
Layer 3	$V_0(0)$ (km/s)	4.5			
	δ	0.1	0.11	0.09	0.01
	ϵ	0.1	0.09	0.09	0.15
	$k_{x1}(\mathrm{s}^{-1})$	0	-0.00	-0.02	0.04
	$\overline{k}_{x2}$ $(\mathrm{s}^{-1}\mathrm{m}^{-1}\times 10^{-5})$	0	0.7		

Table 3. Actual and estimated parameters for the model in Figure 7. The two thin layers are divided into blocks 3 km wide for full MVA and 1.5 km wide in the other two tests. The symmetry-direction velocity V_0 and vertical gradient k_{z1} at location $x=0$ are assumed to be known.

rameters throughout the model. While random traveltime errors are largely suppressed by 2D semblance analysis, the inversion results are sensitive to correlated errors with the spatial period close to spreadlength.

Even in the presence of quadratic lateral velocity variation, the symmetry-direction velocity in thin layers can be constrained by inverting just for V_0 and the lateral gradient k_{x1} (with k_{x2} set to zero) using a block width close to half the effective spreadlength (defined as the maximum distance between the incident and reflected rays at lens depth). Then the algorithm can also recover the anisotropy parameters beneath the laterally heterogeneous overburden. However, when k_{x2} is not taken into account, a block boundary has to be close to the center of the lens. In contrast, layer stripping produces much less accurate results because the moveout for the bottom of a thin LH layer is weakly sensitive to the layer parameters. Also, estimates of the residual moveout from the bottom of thin layers are hampered by waveform distortions, such as the NMO stretch.

The developed algorithm should help build more accurate anisotropic velocity models when the overbur-

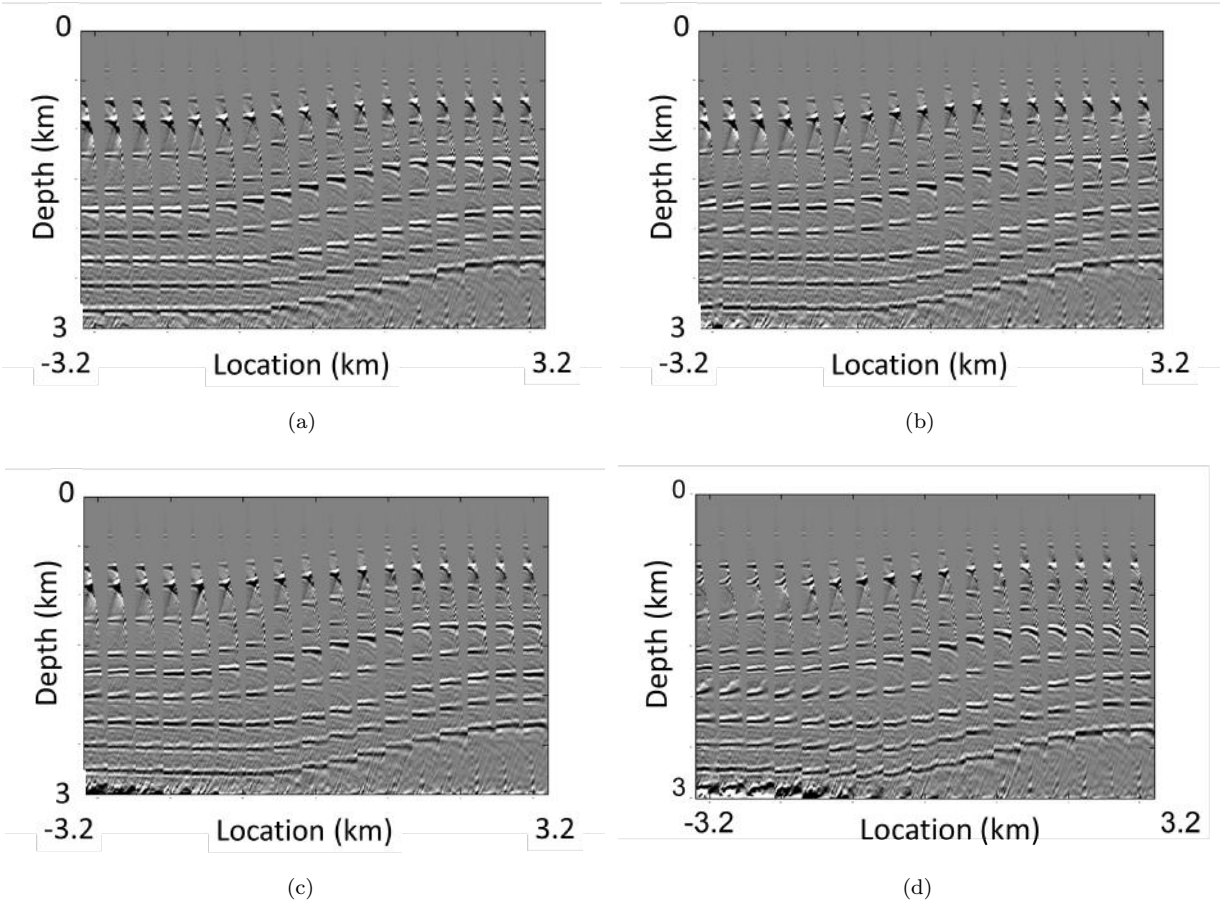

Figure 8. Image gathers for the model from Figure 7 computed using (a) actual model parameters; (b) parameters obtained by our MVA algorithm ("full MVA"), (c) parameters obtained by MVA without taking k_{x2} in the thin layers into account using a block width of 1.5 km; and (d) parameters obtained by MVA in the layer-stripping mode. The estimated parameters of the TTI layers are listed in Table 3. The maximum offset is 4.5 km.

den contains velocity lenses or other types of small-scale lateral heterogeneity. Dividing the model into quasi-factorized blocks makes it possible to avoid instability of parameter estimation typical for reflection tomography.

6 ACKNOWLEDGMENTS

We are grateful to V. Grechka and E. Jenner and to members of the A(nisotropy)-Team of the Center for Wave Phenomena (CWP), Colorado School of Mines (CSM) for helpful discussions. This work was supported by Japan Oil, Gas and Metals National Corporation (JOGMEC) and the Consortium Project on Seismic Inverse Methods for Complex Structures at CWP.

REFERENCES

Al-Chalabi, M., 1979, Velocity determination from seismic reflection data: Applied Science Publishers.

Alkhalifah, T., 1997, Seismic data processing in vertically inhomogeneous TI media: Geophysics, **62**, 662–675.

Alkhalifah, T., and K. Larner, 1994, Migration error in transversely isotropic media: Geophysics, **59**, 1405–1418.

Bakulin, A., Y. K. Liu, O. Zdraveva, and K. Lyons, 2010a, Anisotropic model building with wells and horizons: Gulf of Mexico case study comparing different approaches: The Leading Edge, **29**, 1450–1460.

Bakulin, A., M. Woodward, D. Nichols, K. Osypov, and O. Zdraveva, 2010b, Building tilted transversely isotropic depth models using localized anisotropic tomography with well information: Geophysics, **75**, no. 4, D27–D36.

——— 2010c, Localized anisotropic tomography with

well information in VTI media: Geophysics, **75**, no. 5, D37–D45.

Behera, L., and I. Tsvankin, 2009, Migration velocity analysis for tilted TI media: Geophysical Prospecting, **57**, 13–26.

Biondi, B., 2007, Angle-domain common-image gathers from anisotropic migration: Geophysics, **72**, no. 2, S81–S91.

Blias, E., 2009, Stacking velocities in the presence of overburden velocity anomalies: Geophysical Prospecting, **57**, 323–341.

Calvert, A., E. Jenner, R. Jefferson, R. Bloor, N. Adams, R. Ramkhelawan, and C. S. Clair, 2008, Preserving azimuthal velocity information: Experiences with cross-spread noise attenuation and offset vector tile PreSTM: 78th Annual International Meting, SEG, Expanded Abstracts, 207-211.

Contreras, A. J., and R. B. Latimer, 2010, Acoustic impedance as a sequence stratigraphic tool in structurally complex deepwater settings: The Leading Edge, **29**, 1072–1082.

Grechka, V., 1998, Transverse isotropy versus lateral heterogeneity in the inversion of P-wave reflection traveltimes: Geophysics, **63**, 204–212.

Grechka, V., and I. Tsvankin, 1998, Feasibility of nonhyperbolic moveout inversion in transversely isotropic media: Geophysics, **63**, 957–969.

——— 1999, 3-D moveout inversion in azimuthally anisotropic media with lateral velocity variation: Theory and a case study: Geophysics, **64**, 1202–1218.

Huang, T., S. Xu, J. Wang, G. Ionescu, and M. Richardson, 2008, The benefit of TTI tomography for dual azimuth data in Gulf of Mexico, 222-226: 78th Annual International Meting, SEG, Expanded Abstracts.

Juhlin, C., 1995, Finite-difference elastic wave propagation in 2D heterogeneous transversely isotropic media: Geophysical Prospecting, **43**, 843–858.

Neal, S. L., N. R. Hill, and Y. Wang, 2009, Anisotropic velocity modeling and prestack gaussian-beam depth migration with applications in the deepwater Gulf of Mexico: The Leading Edge, **28**, 1110–1119.

Sarkar, D., and I. Tsvankin, 2003, Analysis of image gathers in factorized VTI media: Geophysics, **68**, 2016–2025.

——— 2004, Migration velocity analysis in factorized VTI media: Geophysics, **69**, 708–718.

——— 2006, Anisotropic migration velocity analysis: Application to a data set from West Africa: Geophysical Prospecting, **54**, 575–587.

Takanashi, M., M. Fujimoto, and D. Chagalov, 2009, Overburden heterogeneity effects in migration velocity analysis: A case study in an offshore Australian field: 71st Annual Internatinal Meeting, EAGE, Extended Abstracts.

Takanashi, M., and I. Tsvankin, 2010, Correction for the influence of velocity lenses on nonhyperbolic moveout inversion for VTI media: 80th Annual International Meting, SEG, Expanded Abstracts, **29**, 238–242.

——— 2011a, Moveout inversion of wide-azimuth data in the presence of velocity lenses: CWP report.

——— 2011b, NMO ellipse for a stratified medium with laterally varying velocity: CWP report.

Toldi, J., 1989, Velocity analysis without picking: Geophysics, **54**, 191–199.

Tsvankin, I., J. Gaiser, V. Grechka, M. van der Baan, and L. Thomsen, 2010, Seismic anisotropy in exploration and reservoir characterization: An overview: Geophysics, **75**, no. 5, 75A15–75A29.

van Hoek, T., S. Gesbert, and J. Pickens, 2010, Geometric attributes for seismic stratigraphic interpretation: The Leading Edge, **29**, 1056–1065.

Červený, V., 1989, Ray tracing in factorized anisotropic inhomogeneous media: Geophysical Journal International, **99**, 91–100.

Wang, X., and I. Tsvankin, 2009, Estimation of interval anisotropy parameters using velocity-independent layer stripping: Geophysics, **74**, no. 5, WB117–WB127.

——— 2010, Stacking-velocity inversion with borehole constraints for tilted TI media: Geophysics, **75**, no. 5, D69–D77.

Woodward, M. J., D. Nichols, O. Zdraveva, P. Whitfield, and T. Johns, 2008, A decade of tomography: Geophysics, **73**, no. 5, VE5–VE11.